CARBON 94 (2015) 531–538

Contents lists available at ScienceDirect

CARBON

journal homepage: www.elsevier.com/locate/carbon

Reduced graphene oxide enhances horseradish peroxidase stability by serving as radical scavenger and redox mediator

Chengdong Zhang [a,*], Silong Chen [a], Pedro J.J. Alvarez [b], Wei Chen [a]

[a] College of Environmental Science and Engineering, Ministry of Education Key Laboratory of Pollution Processes and Environmental Criteria, Tianjin Key Laboratory of Environmental Remediation and Pollution Control, Nankai University, Tianjin 300071, China
[b] Dept. of Civil and Environmental Engineering, Rice University, Houston, TX 77005, USA

ARTICLE INFO

Article history:
Received 14 May 2015
Received in revised form 5 July 2015
Accepted 8 July 2015
Available online 9 July 2015

ABSTRACT

Graphene-based nanomaterials have been widely studied as high-performance matrices for enzyme immobilization and in the development of biosensors. Surface O-functionalities of graphene induce changes in chemical reactivity and electronic conductivity of nanomaterials and may interfere with enzymatic processes; however, the mechanisms are not fully understood. We compare the effects of three commercially available graphene-based nanomaterials, namely a graphene, a graphene oxide (GO), and a reduced graphene oxide (RGO), on the activity/stability of horseradish peroxidase. Both graphene and GO significantly reduced enzyme stability by altering enzyme conformation, which was evidenced by circular dichroism spectroscopy. However, RGO improved enzyme stability up to 7-fold. This increased stability was attributed to the capability of RGO to quench superoxide radicals, which were primarily responsible for the enzyme deactivation. The basal plane of RGO, mainly through quinone moieties, may act as a redox mediator to facilitate enzymatic turnover. Overall, the radical scavenging plus redox mediating capabilities of RGO suggest the potential for graphene-based nanomaterials to enhance enzyme engineering and enzyme-based sensors.

1. Introduction

Graphene and its derivatives (e.g., graphene oxide (GO) and reduced graphene oxide (RGO)) exhibit unique chemical, electronic, thermal, optical and mechanical properties that enable diverse applications in nanobiotechnology, such as nano-biocatalysis, drug delivery, cellular imaging, biomedicine, and biosensing [1–5]. Graphene-based materials have shown great promise as high-performance matrices for enzyme immobilization [4,6], offering advantages such as large surface area, tailor-made surface functionalities and easy substrate accessibility [7,8].

The effectiveness of graphene-based materials in supporting biocatalysis is strongly dependent on the physicochemical properties of the nanomaterials [9,10]. First, the type and distribution of surface functionalities of nanomaterials strongly affect the interactions between nanomaterials and enzymes, and consequently, the structural conformation of and substrate accessibility to adsorbed enzymes. It has been shown that electrostatic interactions are the primary driving force for the adsorption of cytochrome c to GO, whereas hydrophobic effects are the predominant mechanism for its adsorption to RGO. Different interactions had different effects on substrate accessibility to the heme, resulting in either an increase or a decrease in enzyme activity of cytochrome c [11]. Second, different degrees of surface functionalization can also lead to differences in electronic conductivity of graphene-based nanomaterials. Graphene is an electrical conductor, whereas GO can be electrically insulating [12]. For RGO, the π electron network of graphene is partially restored, and the conductivity of RGO can be higher than that of GO [13,14]. It was reported that conductive RGO and graphene have higher oxidation capacities for glutathione and induce more severe oxidative stress in cells than insulating GO [15]. Third, during functionalization, graphenic edges and defects may be induced on the graphene basal surface, which results in high chemical/electrochemical reactivity. In comparison with GO, RGO possessed more abundant edges and defects, and accelerated nitrobenzene reduction [16] and hydroquinone oxidation [17]. However, some features of graphene-based nanomaterials that could enhance biocatalysis have not been explored. For example, RGO can remove hydroxyl and dithiocyanate radicals [12,18], which suggests its potential application as antioxidant to protect enzymes from inactivation. Reactive oxygen species derived from both endogenous biological processes and exogenous sources are primarily responsible for enzyme oxidation [7] and loss of enzyme activity. Albeit, the antioxidant capability of RGO may be

* Corresponding author.
E-mail address: zhangchengdong@nankai.edu.cn (C. Zhang).

http://dx.doi.org/10.1016/j.carbon.2015.07.036
0008-6223/

influenced by the abundance and type of surface O-functionalities, which also affect its physicochemical properties such as reactivity, conductivity, adsorption capacity and suspendability. Moreover, RGO is rich in quinoid-like groups, which can assist electron transfer and activation of molecules in chemical reductions [16]. Therefore, some quinoid structures might also facilitate enzyme-catalyzed redox processes.

The objective of this study was to advance our mechanistic understanding of how functionalization of graphene-based nanomaterials affects enzyme activity and stability. Using three commercially available graphene-based materials, including a graphene, a GO and a RGO, and horseradish peroxidase (HRP) as a model enzyme, we found that both graphene and GO reduced enzyme activity/stability via strong adsorption, whereas RGO improved stability up to 7-fold via acting as radical quencher and redox mediator.

2. Materials and methods

2.1. Materials

GO and RGO were purchased from Plan Nano Materials Tech. Co. (Tianjin, China). Graphene was purchased from XF Nano Materials Tech. Co. (Nanjing, China). GO and RGO were synthesized by Yongsheng Chen's group as detailed previously [19,20]. Graphene was synthesized via chemical exfoliation followed by thermo reduction. Horseradish peroxidase (EC 1.11.1.7, from *Armoracia rusticana*, sigma Type IV, with activity of 250 U/mg), superoxide dismutase (SOD, EC 1.15.1.1, from bovine erythrocytes, with activity of 3000 U/mg), isopropyl alcohol (purity > 99%), benzoquinone (purity > 98%), and 2,2′-azino-bis-(3-ethylbenzthiazoline-6-sulfonic acid) (ABTS, purity > 98%) were purchased from Sigma–Aldrich (China). All other chemicals and solvents used were of analytical grade or higher.

The surface elemental compositions of graphene-based nanomaterials were determined by X-ray photoelectron spectroscopy (XPS) (PHI-5000 Versa Probe, Japan). The ζ potentials were measured by electrophoretic mobility using a ZetaPALS (Brookhaven Instruments, Holtsville, USA). The XPS spectra are provided in the Supporting Information (Fig. S2), and the physicochemical properties of the nanomaterials are summarized in Table 1.

2.2. Incubation of graphene-based nanomaterials with HRP and H_2O_2

Stock suspensions of the graphene-based nanomaterials were prepared by adding nanomaterials to deionized water to a final concentration of 200 mg/L. To increase the dispersion, each suspension was ultrasonicated (150 W, 40 kHz) for 4 h immediately prior to the beginning of experiments. Although sonication can lead to the formation of radicals, spectroscopic analysis showed that this sonication process did not lead to HRP oxidation (Fig. S1). The HRP stock solution (1.5 mg/mL) was prepared by dissolving enzyme in 10 mM phosphate buffer solution (PBS) at pH 5.0 (the optimum pH for HRP) immediately before use. The nanomaterial stock suspensions were further diluted with PBS buffer (10 mM, pH 5.0) to obtain the desired concentrations. The enzyme stock solution was then added to the nanomaterial suspension to give a total volume of 15 mL containing 15 mg/L HRP and 0, 5, 25 or 50 mg/L nanomaterials. The reaction was initiated by adding 100 μL of 2.25 mM H_2O_2 solution, and the final concentration of H_2O_2 was 15 μM. An aliquot of 100 μL of 2.25 mM H_2O_2 was added daily. All samples were stored in the dark and shaken at 160 rpm at 28 °C. At appropriate time intervals, samples were withdrawn to obtain various measurements. All samples were prepared in triplicate, and samples containing HRP alone without daily addition of H_2O_2 were also prepared to monitor activity loss. When required, 0.5 mM of isopropyl alcohol or 1 mM of benzoquinone was added to the reaction mixture at the beginning. No benzoquinone degradation by HRP was observed during incubation (see SI). Both isopropyl alcohol [21] and benzoquinone [22] were added in excess of potential radical production in the reaction system.

For experiments involving SOD, an SOD solution (prepared in PBS buffer) was added to the above HRP reaction system at a final concentration of 15 mg/L at the beginning of the reaction. Due to a rapid loss of activity, 100 μL of SOD stock solution (1.5 mg/mL) was added to the mixture daily. SOD was added in excess to efficiently remove superoxide anions [23,24].

2.3. Enzyme activity assays

HRP activity was determined by monitoring the oxidation of ABTS to its cation radical at 420 nm [25]. Briefly, 100-μL samples were removed at predetermined times and immediately diluted 10-fold in 10 mM PBS (pH 5.0). Then, 100 μL of the diluted solution was added to a quartz cuvette, followed by the addition of 900 μL of 5 mM ABTS (prepared in 10 mM PBS at pH 5.0) and 100 μL of 0.1 M H_2O_2 to start the assay. The change in absorbance was examined every 2 s over a period of 1 min at 420 nm using a UV–vis spectrometer (TU-1810, Persee Co., China). The interference of the nanomaterials with the activity assays was negligible (see SI).

The decay in enzyme activity, expressed as the ratio of the activity A_t at given time to the initial activity A_0, is described by bi-exponential equation with k_1 and k_2 as the rate constants [26]:

$$\frac{A_t}{A_0} = \alpha \cdot \exp(-k_1 t) + \beta \cdot \exp(-k_2 t)$$

This bi-exponential model has been widely used to describe the kinetics of enzyme deactivation, especially in the context of biotechnology [26]. The half-life ($t_{1/2}$) is defined as the time taken for the loss of 50% of original activity.

Table 1
Elemental compositions and ζ potential of the nanomaterials.

Nanomaterial	C (%)[a]				O (%)[a]	C:O ratio	ζ Potential (mV)[bc]
	C—C/C=C	C—OH	C—O—C	C=O			
GO	29.04	2.66	27.06	7.44	31.63	2.09	−31.62 ± 1.18
Graphene	58.21	16.45	7.42	8.46	8.86	10.26	–[d]
RGO	41.58	22.54	1.93	17.70	12.33	6.79	−20.96 ± 0.99
RGO-88 h [e]	36.05	19.48	1.28	18.84	20.74	3.64	–

[a] Analyzed by X-ray photoelectron spectroscopy.
[b] Measured by electrophoretic mobility using a Zetasizer.
[c] Values after "±" represent the standard deviation of five replicates.
[d] Due to precipitation, ζ potential cannot be measured properly.
[e] RGO incubated with 15 mg/L HRP and 15 μM H_2O_2 for 88 h.

2.4. Adsorption of HRP onto nanomaterials

Briefly, 2 mL of the nanomaterial suspension (200 mg/L) was added to 4-mL vials. Then, a series of volumes of HRP (1000 mg/L) solution prepared in 0.2 M phosphate buffer (pH 5.0) were added to the vials, and phosphate buffer was added to achieve total volumes of 4 mL. The final enzyme concentrations were 50 mg/L, 75 mg/L, 150 mg/L, 300 mg/L and 500 mg/L. The mixture was shaken for 2 h at 160 rpm and 28 °C, and adsorption equilibrium was achieved after 30 min of incubation. The samples were subsequently centrifuged at 11,000 rpm for 20 min at 4 °C. The protein content in the supernatants was determined using the bicinchoninic acid method (BCA) or the μBCA assay [27]. The amount of enzyme loaded onto the nanomaterial was determined by measuring the difference in the enzyme concentration in solution before and after exposure to nanomaterials. All experiments were performed in triplicate.

2.5. Circular dichroism (CD) spectroscopy for HPR secondary structure analysis

The above reaction mixture (containing 15 mg/L HRP, 15 μM H_2O_2 and various concentrations of nanomaterial) was incubated for 2 h, and 3 mL was withdrawn for CD analysis. The CD spectra were obtained on a CD spectrometer model J-715 (JASCO, Japan). The far-UV region was scanned between 195 and 250 nm. The scan speed was 20 nm/min with a bandwidth of 2.0 nm at room temperature. The CD signal was determined as the total signal (protein plus background) minus the background signal (nanomaterial in PBS buffer). Three replicates were performed and averaged for the calculation of secondary structures. The relative contents of secondary structures, including α-helix, β-sheet, β-turn and random coil, were calculated by the Jasco secondary structure estimation software [28].

2.6. Characterization of structural changes of nanomaterials after enzymatic incubation

2.6.1. XPS analysis

After incubation for 88 h, samples were collected by centrifugation at 11,000*g* for 20 min and then washed with deionized water three times. This process efficiently removed adsorbed enzyme, and the absence of protein on the nanomaterial surface was confirmed by the lack of obvious change in the nitrogen content of the nanomaterial before and after exposure to the enzyme (Table S1). The lyophilized nanomaterial was then subjected to XPS analysis.

2.6.2. Raman spectroscopy

After incubation for 88 h, samples were withdrawn and centrifuged at 11,000*g* for 20 min. The precipitate was lyophilized on a freeze dryer (LGJ-18, Beijing Songyuan Scientific Co.). All spectra were collected on a Renishaw inVia Raman microscope using an excitation wavelength of 632.8 nm. Samples were scanned three times from 500 to 3000 cm^{-1} to visualize the D and G bands. Significant differences ($p < 0.05$) in the D:G ratio were determined by one-way ANOVA. All statistical analyses were conducted using Statistical Packages for the Social Sciences (SPSS) Version 19.0.3.

2.7. Analysis of the redox state of HRP by UV–vis absorption spectroscopy

Samples were prepared as described in Section 2.2. At the specified time, 1 mL of sample was withdrawn and scanned in the spectral range of 200–600 nm using a UV–vis spectrometer (TU-1810, Persee Co., China). The spectrum of the corresponding nanomaterial suspension was then subtracted from the sample spectra.

3. Results and discussion

3.1. Characterization of surface O-functionalities of graphene-based nanomaterials

The three graphene-based nanomaterials differ significantly in the type, abundance, and distribution of surface O-functionalities (Table 1 and Fig. S2). The C:O ratio decreased in the order of graphene > RGO > GO. The O-functional groups on GO were primarily epoxy/ether groups, whereas those on RGO were mainly hydroxyl and carbonyl groups (Table 1). The distribution of O-functional groups on graphene was more uniform compared with GO and RGO, with hydroxyl groups accounted for approximately half of the surface O-functionalities and roughly equal amounts of epoxy/ether and carbonyl groups accounted for the rest. The small amounts of surface O-functional groups on graphene were likely due to the incomplete reduction of graphene oxide, the parent product of the commercial graphene. Both GO and RGO were negatively charged (Table 1). The surface charge of graphene could not be measured properly due to precipitate formation.

3.2. Graphene-based nanomaterials show differential effects on enzyme stability

In the absence of graphene-based nanomaterial, the progressive loss of activity of HRP was apparent (Fig. 1), and the half-life of the native enzyme ($t_{1/2}$) was approximately 8.9 h (Table 2). In the presence of graphene or GO, the loss of activity became more rapid. For example, in the presence of 25 mg/L GO or graphene, the $t_{1/2}$ was decreased to 3.06 and 1.78 h, respectively. Interestingly, in the presence of 5, 25 or 50 mg/L RGO, the $t_{1/2}$ of the enzyme increased to 21.3, 52.5, and 59.8 h, respectively, indicating that under the test experimental conditions RGO significantly enhanced the stability of HRP.

3.3. Adsorption of HRP on graphene-based nanomaterials result in secondary structure change

The rapid loss of enzyme activity in the presence of graphene or GO was likely attributable to the strong adsorption of HRP to these two nanomaterials, because adsorption of enzymes onto nanomaterial may result in substantial changes in the secondary structure of enzymes [29]. As shown in Fig. 2, adsorption of HRP on GO and graphene was markedly stronger than on RGO (see the fitted distribution coefficients, K_d, in Table S2). This is in general consistent with the order that the materials induced enzyme unfolding: graphene > GO > RGO. As demonstrated with CD spectra (Fig. S3), adsorption led to decrease in α-helices and increase in β-sheets, β-turns and random coils (Table 3). For example, the α-helical content of the native HRP was 33.3%, but decreased to 26.2% in the presence of 5 mg/L graphene and 29.3% in the presence of 5 mg/L GO. In comparison, the value changed little in the presence of 5 mg/L RGO (33.1%). The same general trend was also observed at higher concentration of nanomaterials (25 mg/L). Apparently, in comparison with RGO, graphene and GO induced larger changes in enzyme structures due to stronger adsorption.

The different effects of the three nanomaterials on HRP stability may also be linked to the specific types of enzyme–nanomaterial interactions. Graphene interacts with HRP primarily through hydrophobic effects and π–π interactions [10], whereas for GO and RGO electrostatic interactions and hydrogen bonding may also

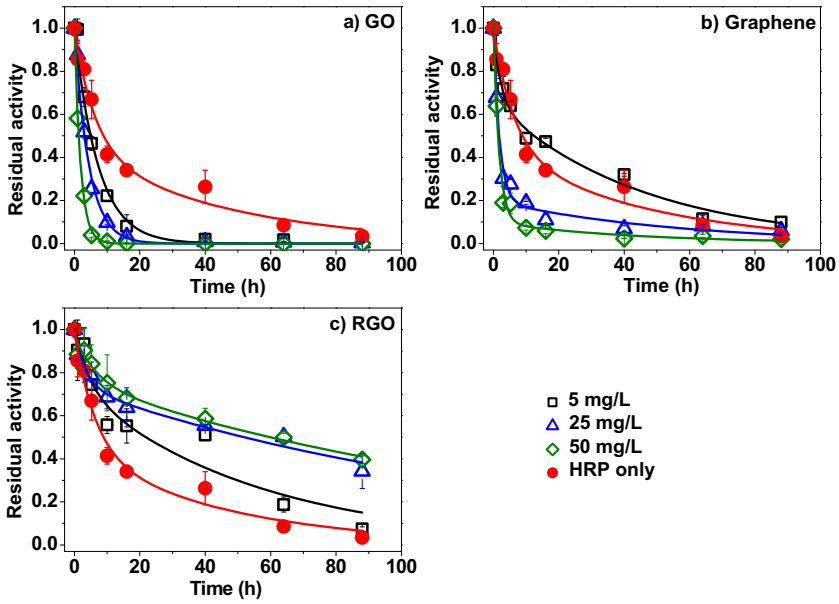

Fig. 1. Effects of 5, 25, or 25 mg/L of graphene oxide (GO), graphene, and reduced graphene oxide (RGO) on the stability of HRP as a function of time. The reaction mixtures contained 15 mg/L HRP and 15 μM H_2O_2. Residual activity was expressed as the activity at respective time versus the initial activity of HRP alone. Error bars represent standard deviations of triplicates.

Table 2
Summary of model fitting parameters and calculated half-lives ($t_{1/2}$).

Equation $\frac{A_t}{A_0} = \alpha \cdot \exp(-k_1 t) + \beta \cdot \exp(-k_2 t)$							
Nanomaterial	Nanomaterial concentration (mg/L)[b]	α	k_1	β	k_2	$t_{1/2}$ (h^{-1})	R^2
GO	5	1.000	0.139	–[a]	–[a]	4.98	0.985
	25	1.000	0.227	–[a]	–[a]	3.06	0.992
	50	1.000	0.531	–[a]	–[a]	1.31	0.999
G	5	0.656	0.022	0.332	0.432	12.51	0.984
	25	0.806	0.543	0.198	0.018	1.78	0.985
	50	0.912	0.582	0.098	0.023	1.61	0.985
RGO	5	0.265	0.224	0.741	0.018	21.27	0.906
	25	0.247	0.269	0.735	0.007	52.48	0.971
	50	0.764	0.007	0.210	0.155	59.79	0.975
HRP	0	0.449	0.022	0.544	0.160	8.90	0.972
SOD	0	0.288	1.075	0.712	0.009	39.48	0.988
BQ	0	1.000	0.005	–[a]	–[a]	133.74	0.997

[a] The value of β of the fitting curve was zero.
[b] The initial H_2O_2 concentration was 15 μM in all cases.

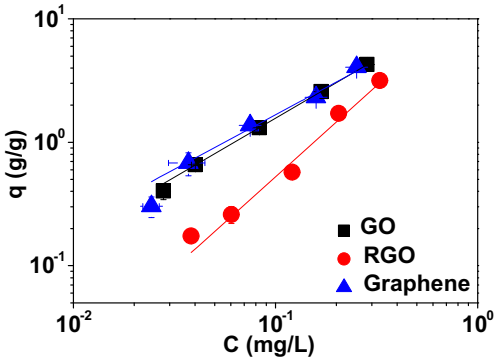

Fig. 2. The adsorption isotherms of HRP on graphene-based nanomaterials at pH 5.0 in 0.1 M phosphate buffer. Error bars, in some cases smaller than the symbols, represent standard deviations of triplicates.

play significant roles, because of these two nanomaterials contain greater amounts of O-containing functional groups [4,30]. When hydrophobic effects are the predominant driving force for adsorption, soluble proteins, which often do not have surface-exposed hydrophobic residues, undergo conformational changes to facilitate adsorption [4], which was evidenced by the large structural change of HRP on graphene (Table 3). Electrostatic interactions and hydrogen bonding between functionalized nanomaterials and enzymes could decrease hydrophobic-induced denaturation [31], which explains the lesser extent of structural change on RGO and GO (Table 3). An interesting observation was that similar enzyme structural changes (albeit to a lesser extent) were observed in the presence of RGO (Table 3); however, an increase in enzyme activity/stability was observed. This discrepancy suggests that RGO was capable of preserving HRP activity through other mechanisms which will be discussed below.

Table 3
Adsorption of HRP on graphene-based nanomaterials[a] result in secondary structure change.

Nanomaterial	Nanomaterial conc. (mg/L)	α-helix (%)	β-sheet (%)	β-turn (%)	γ-random (%)	Residual STD (%)
GO	5	29.3 ± 0.6[b]	23.3 ± 0.4	7.6 ± 0.2	39.9 ± 0.2	8.2 ± 0.7
	25	27.3 ± 0.3	24.8 ± 0.7	8.4 ± 2.0	39.5 ± 1.2	9.0 ± 0.2
Graphene	5	26.2 ± 0.7	20.1 ± 0.6	16.2 ± 0.6	38.1 ± 1.1	8.5 ± 0.3
	25	–[c]	–	–	–	>10
RGO	5	33.1 ± 1.1	20.8 ± 1.8	7.5 ± 0.3	38.6 ± 0.6	6.3 ± 0.7
	25	30.8 ± 1.1	22.7 ± 0.6	7.7 ± 1.6	39.0 ± 0.1	7.2 ± 1.0
	50	29.4 ± 0.4	23.0 ± 0.4	8.5 ± 0.4	39.1 ± 1.1	5.9.±0.8
HRP	0	33.3 ± 0.1	20.6 ± 0.9	7.9 ± 0.9	38.3 ± 0.1	4.3 ± 0.4

[a] Reaction conditions: nanomaterial, 15 mg/L HRP and 15 μM H_2O_2 were incubated for 2 h at pH 5.0.
[b] Values after "±" represent the standard deviation of three replicates.
[c] "–" indicates no calculated results because the value of residual STD fitted by the Yang equation was not reasonable.

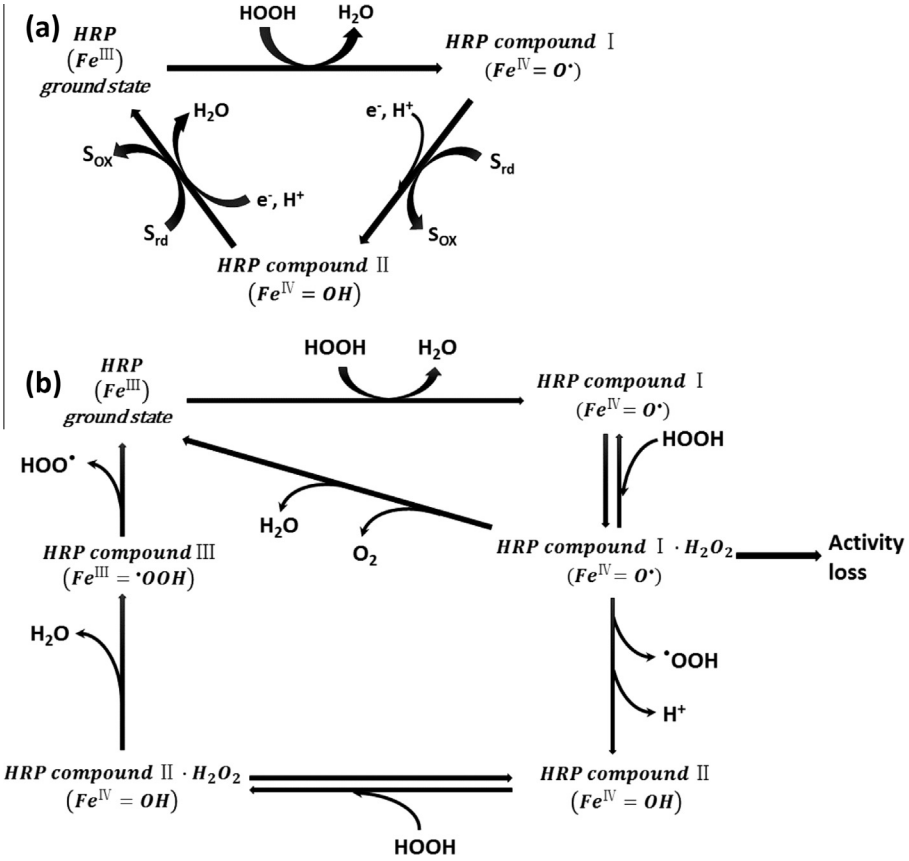

Fig. 3. (a) Catalytic cycle of HRP. (b) Mechanism of HRP inactivation by H_2O_2 (adapted form Ref. [32]). S_{rd} and S_{ox} mean reduced and oxidized substrate, respectively.

3.4. RGO preserves HRP activity by scavenging $O_2^{\bullet-}$ radicals

The catalytic cycle of HRP is initiated by H_2O_2 (Fig. 3a). Meanwhile, HRP undergoes a progressive loss of activity due to the reaction with H_2O_2 (Fig. 3b), and the superoxide anion ($O_2^{\bullet-}$) generated in the series of reactions is responsible for heme destruction, enzyme oxidation and inactivation [32]. We hypothesize that RGO may scavenge $O_2^{\bullet-}$ radicals, and thus, protect enzymes from oxidation. We verified the positive effects of radical scavenging on the stability of HRP using two radical scavengers, and found that adding SOD, a $O_2^{\bullet-}$ scavenger, resulted in an increase in $t_{1/2}$ of more than 3-fold (Fig. 4 and Table 2), whereas no stability enhancement was observed upon the addition of the hydroxyl radical scavenger isopropyl alcohol (Fig. 4).

To further confirm the role of RGO as a radical scavenger, we examined the oxidation of RGO using XPS and Raman spectroscopy. The XPS spectra (Fig. S2) revealed that after 88 h of incubation with HRP, the oxygen content of RGO increased from 12.3% to 20.7%, and the C:O ratio decreased from 6.8 to 3.6 (Table 1). Oxygen-free imperfections in sp^2 carbons may be responsible for the reaction with $O_2^{\bullet-}$ [33,34], leading to the formation of epoxide and hydroxyl functional groups on the surface [35,36].

The tangential G band and disorder-induced D band in Raman spectra are characteristic of graphitic carbon materials, and the D:G height ratio is an index of structural disorder [37]. After incubation with HRP and H_2O_2, the D:G ratios remained unchanged for graphene and GO, whereas RGO exhibited an increased

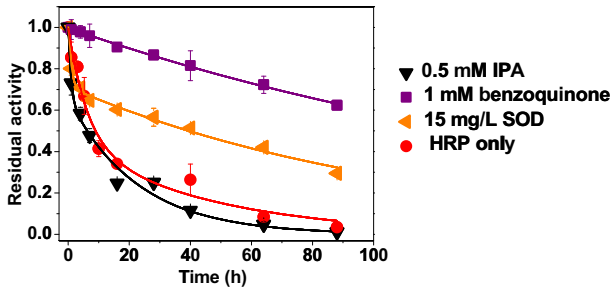

Fig. 4. Enhanced HRP stability by SOD (15 mg/L) and benzoquinone (1 mM) but not by hydroxyl radical scavenger isopropyl alcohol (IPA, 0.5 mM). In all cases, the initial concentration of H_2O_2 was 15 μM and an aliquot of 100 μL of 2.25 mM H_2O_2 was added daily. Error bars represent standard deviations of triplicates.

D:G ratio (the structural changes were not caused by H_2O_2 alone; see Fig. S4). The increase in structural disorder of RGO was attributed to the appearance of holes and wrinkling on the graphene plane from re-oxidation of RGO by free radicals [12]. Note that HRP has been reported to enzymatically oxidize GO [38]. Nonetheless, we did not observe any structural changes in GO. This was likely because of the differences in the materials used (varied physicochemical properties of GO) and reaction conditions (e.g., enzyme and H_2O_2 concentrations) in this and previous studies.

3.5. RGO as mediator for enzymatic turnover

Given the high content of carbonyl and the changes of RGO surface properties (Table 1) upon incubation with HRP, we propose that RGO can also facilitate enzymatic turnover by serving as an electron mediator. A number of studies have indicated that quinoid-like structure can mediate redox process via an electron-shuttling mechanism [39–42]. For example, quinoid redox mediators (anthraquinone-2-sulfonate) facilitate the reduction of azo dyes by anaerobic bacteria [22]. Likely, because of its high amounts of quinoid-like groups, RGO facilitates electron transfer in nitrobenzene reduction by sulfide [16]. We propose that quinoid-like groups on RGO may also facilitate enzyme activity/stability via the following mechanisms (a conceptual scheme is shown in Fig. 5). First, quinones can consume $O_2^{\cdot-}$ radical effectively [43] by one-electron reduction to the corresponding semiquinone radicals or two-electron reduction to hydroquinone. Second, as a substrate of HRP [44], hydroquinone can be oxidized to semiquinone and quinone, releasing electrons to facilitate the reductive conversion of HRP back to the ground state. Third, the high electrical conductivity makes RGO a super mediator for electron transfer [45,46].

This mediating effect of RGO as electron donor can be visualized by monitoring the changes in the Soret absorption of HRP by UV–vis spectroscopy (Fig. 6), because the position of the Soret band reflects the coordination and spin state of the heme [47]. The catalytic cycle of HPR (Fig. 3a) show the oxidative status of heme change from ground state (oxidative + 3) to compound I (oxidative + 5), then to compound II (oxidative + 4), and finally back to ground state. Inactive enzyme, compound III, may also form while reacting with excess H_2O_2 (Fig. 3b). The UV–vis spectra of ground state HRP was characterized by a Soret region at 403 nm [47] (Fig. 6a), and the adsorption peak remained stable during incubation. After the addition of H_2O_2, the peak exhibited a red shift to 418 nm, and the peak intensity decreased progressively with time (Fig. 6b). Compounds II and III were characterized by adsorptions at 420 nm and 418 nm, respectively [48], indicating that H_2O_2 inactivated HRP by converting it to oxidized Compound III, and the enzyme conformation denatured gradually with time. In the presence of 25 mg/L GO, HRP remained oxidized, and no mediating effect was observed (Fig. 6c). However, in the presence of 25 mg/L RGO, the Soret absorbance peak first exhibited a red shift to 418 nm, followed by a blue shift to 400 nm over 3 h (Fig. 6d), and the peak was still detectable after 88 h of incubation. The spectral shift as a function of time (Fig. 6e) revealed the assistance of RGO as an electron donor in converting HRP Compound III to the ground state. A small blue shift (3 nm) in the Soret maximum absorbance indicated a decrease in the non-planarity of the porphyrin ring in the heme groups [49], possibly due to the interaction with RGO.

We also added 1 mM benzoquinone as a surrogate to evaluate the effect of quinoid-like groups in mediating enzyme activity. Benzoquinone can act as both an $O_2^{\cdot-}$ radical quencher and a redox mediator, whereas SOD is only effective in $O_2^{\cdot-}$ removal. The reaction rate constant of benzoquinone with $O_2^{\cdot-}$ ($1 \times 10^9\ M^{-1}\ s^{-1}$) [50] is comparable to that of SOD ($2.4 \times 10^9\ M^{-1}\ s^{-1}$) [51]. However, the enhancement of enzyme activity/stability was more pronounced for benzoquinone, with an estimated $t_{1/2}$ of 133.7 h (Fig. 2 and Table 2). As expected, benzoquinone accelerated the enzymatic turnover from the oxidative state (418 nm) to the ground state (403 nm) (Fig. S5). Hence, the contribution of the quinoid-like structure as a redox mediator in facilitating

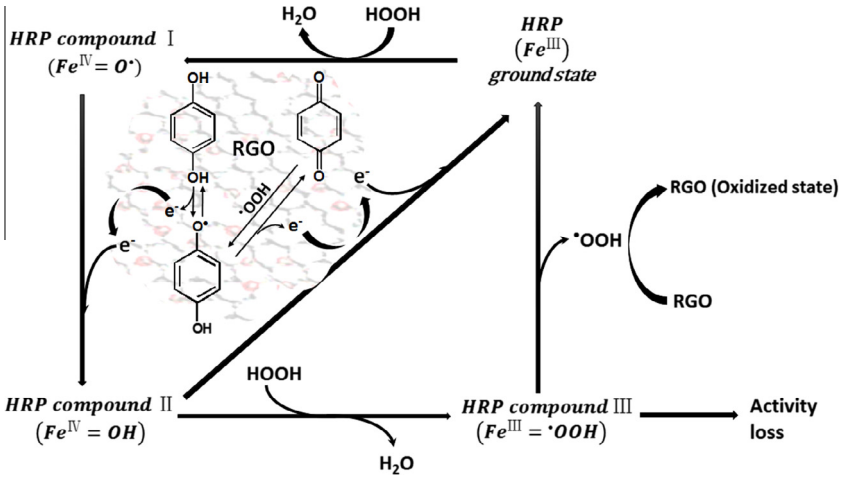

Fig. 5. Proposed mechanisms for the roles of RGO in maintaining HRP stability.

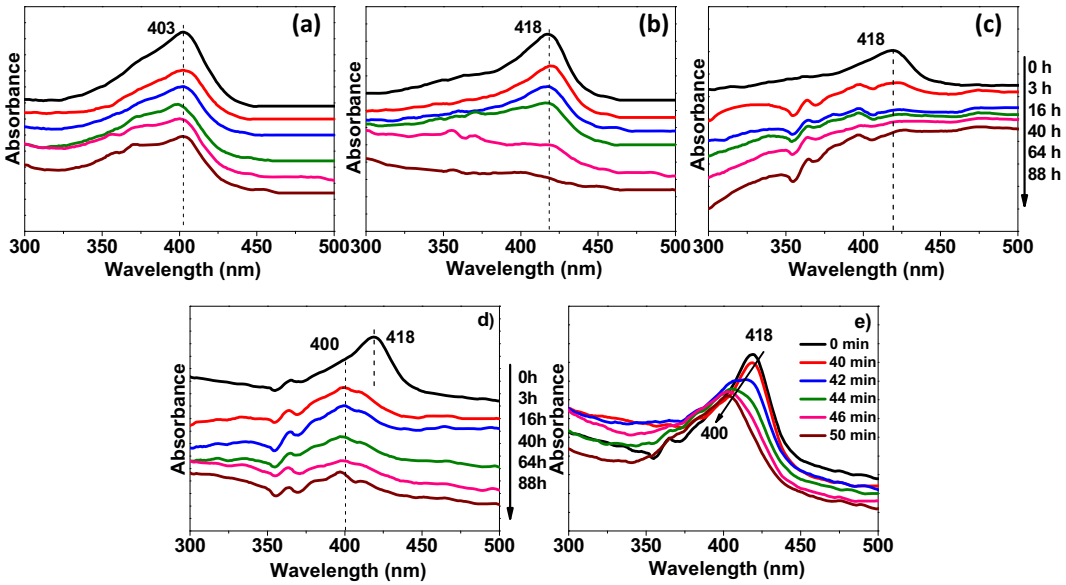

Fig. 6. Changes in UV–vis spectra of HRP upon incubation with different nanomaterials as a function of time: (a) HRP only; (b) HRP with 15 μM H_2O_2; (c) HRP with 25 mg/L GO and 15 μM H_2O_2; and (d and e) HRP with 25 mg/L RGO and 15 μM H_2O_2 (UV–vis spectra of plot (e) were collected within the first hour of the experiment). HRP concentrations were 15 mg/L in all cases.

enzyme activity is appreciable. Nevertheless, quinone redox chemistry is highly sensitive to the quinoid structure. Therefore, further studies with RGO functionalized by different types of quinone groups (and varying extent of functionalization) are needed to discern the importance of these structures and enable material design.

An important implication of this study is that graphene-based nanomaterials with the above-mentioned structural characteristics may also interfere with microbial respiration or extracellular electron transfer processes, thus altering metabolic pathways or causing toxicity. The effects of graphene-based nanomaterials on intracellular or extracellular electron-transfer processes have not been fully explored.

4. Conclusions

RGO exerts versatile functions in mediating enzyme activity/stability. Thus, such graphene-based nanomaterials could not only be used as matrix for enzyme immobilization but also as solid-state electron mediators with tunable surface functionality. The key factor that enables efficient enzyme loading and electron transfer in a quinoid-like system lies in achieving a balance between the degree of GO reduction (for conductivity restoration and retaining chemical activity) and the level of hydrophobicity (for good dispensability and enzyme structure maintaining). By further discerning the link between the functionalization of graphene-based nanomaterials and their effect on enzymatic process, we may be able to broaden nanotechnology applications in biotechnology.

Acknowledgments

This work was supported by the National Science Fund for Distinguished Young Scholars (Grant 21425729), the Ministry of Science and Technology of China (Grant 2014CB932001), the National Science Foundation of China (Grants 81373039 and 21237002), and the Tianjin Municipal Science and Technology Commission (Grant 13JCZDJC35900).

Appendix A. Supplementary data

Supplementary data associated with this article can be found, in the online version, at http://dx.doi.org/10.1016/j.carbon.2015.07.036.

References

[1] S.K. Vashist, J.H.T. Luong, Recent advances in electrochemical biosensing schemes using graphene and graphene-based nanocomposites, Carbon 84 (2015) 519–550.
[2] H. Wu, H. Shi, Y. Wang, X. Jia, C. Tang, J. Zhang, et al., Hyaluronic acid conjugated graphene oxide for targeted drug delivery, Carbon 69 (2014) 379–389.
[3] Q. Fang, Y. Shen, B. Chen, Synthesis, decoration and properties of three-dimensional graphene-based macrostructures: a review, Chem. Eng. J. 264 (2015) 753–771.
[4] I.V. Pavlidis, M. Patila, U.T. Bornscheuer, D. Gournis, H. Stamatis, Graphene-based nanobiocatalytic systems: recent advances and future prospects, Trends Biotechnol. 32 (2014) 312–320.
[5] J. Liu, Z. Liu, C.J. Barrow, W. Yang, Molecularly engineered graphene surfaces for sensing applications: a review, Anal. Chim. Acta 859 (2015) 1–19.
[6] P. Liang, H. Bao, J. Yang, L. Zhang, G. Chen, Preparation of porous graphene oxide–poly(urea–formaldehyde) hybrid monolith for trypsin immobilization and efficient proteolysis, Carbon 97 (2016) 25–34.
[7] A.S. Campbell, C. Dong, F. Meng, J. Hardinger, G. Perhinschi, N. Wu, et al., Enzyme catalytic efficiency: a function of bio–nano interface reactions, ACS Appl. Mater. Interfaces 6 (2014) 5393–5403.
[8] J. Zhang, F. Zhang, H. Yang, X. Huang, H. Liu, J. Zhang, et al., Graphene oxide as a matrix for enzyme immobilization, Langmuir 26 (2010) 6083–6085.
[9] T. Mesarič, L. Baweja, B. Drašler, D. Drobne, D. Makovec, P. Dušak, et al., Effects of surface curvature and surface characteristics of carbon-based nanomaterials on the adsorption and activity of acetylcholinesterase, Carbon 62 (2013) 222–232.
[10] V.C. Sanchez, A. Jachak, R.H. Hurt, A.B. Kane, Biological interactions of graphene-family nanomaterials: an interdisciplinary review, Chem. Res. Toxicol. 25 (2012) 15–34.
[11] X. Yang, C. Zhao, E. Ju, J. Ren, X. Qu, Contrasting modulation of enzyme activity exhibited by graphene oxide and reduced graphene, Chem. Commun. 49 (2013) 8611.
[12] J.G. Radich, P.V. Kamat, Making graphene holey. Gold-nanoparticle-mediated hydroxyl radical attack on reduced graphene oxide, ACS Nano 7 (2013) 5546–5557.
[13] M.M. Storm, M. Overgaard, R. Younesi, N.E.A. Reeler, T. Vosch, U.G. Nielsen, et al., Reduced graphene oxide for Li–air batteries: the effect of oxidation time and reduction conditions for graphene oxide, Carbon 85 (2015) 233–244.
[14] A. Ambrosi, C.K. Chua, A. Bonanni, M. Pumera, Electrochemistry of graphene and related materials, Chem. Rev. 114 (2014) 7150–7188.

[15] S. Liu, T.H. Zeng, M. Hofmann, E. Burcombe, J. Wei, R. Jiang, et al., Antibacterial activity of graphite, graphite oxide, graphene oxide, and reduced graphene oxide: membrane and oxidative stress, ACS Nano 5 (2011) 6971–6980.
[16] H. Fu, D. Zhu, Graphene oxide-facilitated reduction of nitrobenzene in sulfide-containing aqueous solutions, Environ. Sci. Technol. 47 (2013) 4204–4210.
[17] C. Li, L. Li, L. Sun, Z. Pei, J. Xie, S. Zhang, Transformation of hydroquinone to benzoquinone mediated by reduced graphene oxide in aqueous solution, Carbon 89 (2015) 74–81.
[18] R. Chadha, N. Biswas, G.B. Markad, S.K. Haram, T. Mukherjee, S. Kapoor, Interaction of reduced graphene oxide with free radicals and silver clusters, Chem. Phys. Lett. 529 (2012) 54–58.
[19] H.A. Becerril, J. Mao, Z. Liu, R.M. Stoltenberg, Z. Bao, Y. Chen, Evaluation of solution-processed reduced graphene oxide films as transparent conductors, ACS Nano 2 (2008) 463–470.
[20] L. Zhang, J. Liang, Y. Huang, Y. Ma, Y. Wang, Y. Chen, Size-controlled synthesis of graphene oxide sheets on a large scale using chemical exfoliation, Carbon 47 (2009) 3365–3368.
[21] S. Hwang, S.G. Huling, S. Ko, Fenton-like degradation of MTBE: effects of iron counter anion and radical scavengers, Chemosphere 78 (2010) 563–568.
[22] J. Rau, H.-J. Knackmuss, A. Stolz, Effects of different quinoid redox mediators on the anaerobic reduction of azo dyes by bacteria, Environ. Sci. Technol. 36 (2002) 1497–1504.
[23] M.K. Beissenhirtz, F.W. Scheller, M.S. Viezzoli, F. Lisdat, Engineered superoxide dismutase monomers for superoxide biosensor applications, Anal. Chem. 78 (2006) 928–935.
[24] Z. Ai, Z. Gao, L. Zhang, W. He, J.J. Yin, Core–shell structure dependent reactivity of Fe@Fe_2O_3 nanowires on aerobic degradation of 4-chlorophenol, Environ. Sci. Technol. 47 (2013) 5344–5352.
[25] Q. Huang, W.J. Weber, Peroxidase-catalyzed coupling of phenol in the presence of model inorganic and organic solid phases, Environ. Sci. Technol. 38 (2004) 5238–5245.
[26] C. Aymard, A. Belarbi, Kinetics of thermal deactivation of enzymes: a simple three parameters phenomenological model can describe the decay of enzyme activity, irrespectively of the mechanism, Enzyme Microb. Technol. 27 (2000) 612–618.
[27] R. Pang, M. Li, C. Zhang, Degradation of phenolic compounds by laccase immobilized on carbon nanomaterials: diffusional limitation investigation, Talanta 131 (2015) 38–45.
[28] J.T. Yang, C.-S.C. Wu, H.M. Martinez, Calculation of protein conformation from circular dichroism, in: C.H.W. Hirs, S.N. Timasheff (Eds.), Methods in Enzymology, Academic Press, 1986, pp. 208–269.
[29] X.L. Wei, Z.Q. Ge, Effect of graphene oxide on conformation and activity of catalase, Carbon 60 (2013) 401–409.
[30] Y. Zhang, C. Wu, S. Guo, J. Zhang, Interactions of graphene and graphene oxide with proteins and peptides, Nanotechnol. Rev. 2 (2013) 27–45.
[31] C. Zhang, S. Luo, W. Chen, Activity of catalase adsorbed to carbon nanotubes: effects of carbon nanotube surface properties, Talanta 113 (2013) 142–147.
[32] J. Hernández-Ruiz, M.B. Arnao, A.N. Hiner, F. García-Cánovas, M. Acosta, Catalase-like activity of horseradish peroxidase: relationship to enzyme inactivation by H_2O_2, Biochem. J. 354 (2001) 107–114.
[33] E.Y. Kataev, D.M. Itkis, A.V. Fedorov, B.V. Senkovsky, D.Y. Usachov, N.I. Verbitskiy, et al., Oxygen reduction by lithiated graphene and graphene-based materials, ACS Nano 9 (2015) 320–326.
[34] Y. Qiu, Z. Wang, A.C.E. Owens, I. Kulaots, Y. Chen, A.B. Kane, et al., Antioxidant chemistry of graphene-based materials and its role in oxidation protection technology, Nanoscale 6 (2014) 11744–11755.
[35] D.M. Itkis, D.A. Semenenko, E.Y. Kataev, A.I. Belova, V.S. Neudachina, A.P. Sirotina, et al., Reactivity of carbon in lithium–oxygen battery positive electrodes, Nano Lett. 13 (2013) 4697–4701.
[36] H. Gao, W. Chen, J. Yuan, Z. Jiang, G. Hu, W. Shangguan, et al., Controllable O_2^- oxidization graphene in TiO_2/graphene composite and its effect on photocatalytic hydrogen evolution, Int. J. Hydrogen Energy 38 (2013) 13110–13116.
[37] C. Zhang, W. Chen, P.J.J. Alvarez, Manganese peroxidase degrades pristine but not surface-oxidized (carboxylated) single-walled carbon nanotubes, Environ. Sci. Technol. 48 (2014) 7918–7923.
[38] G.P. Kotchey, B.L. Allen, H. Vedala, N. Yanamala, A.A. Kapralov, Y.Y. Tyurina, et al., The enzymatic oxidation of graphene oxide, ACS Nano 5 (2011) 2098–2108.
[39] H. Zhang, E.J. Weber, Elucidating the role of electron shuttles in reductive transformations in anaerobic sediments, Environ. Sci. Technol. 43 (2009) 1042–1048.
[40] D.T. Scott, D.M. McKnight, E.L. Blunt-Harris, S.E. Kolesar, D.R. Lovley, Quinone moieties act as electron acceptors in the reduction of humic substances by humics-reducing microorganisms, Environ. Sci. Technol. 32 (1998) 2984–2989.
[41] E.J. O'Loughlin, Effects of electron transfer mediators on the bioreduction of lepidocrocite (γ-FeOOH) by shewanella putrefaciens CN32, Environ. Sci. Technol. 42 (2008) 6876–6882.
[42] J. Jiang, I. Bauer, A. Paul, A. Kappler, Arsenic redox changes by microbially and chemically formed semiquinone radicals and hydroquinones in a humic substance model quinone, Environ. Sci. Technol. 43 (2009) 3639–3645.
[43] R.I. Samoilova, A.R. Crofts, S.A. Dikanov, Reaction of superoxide radical with quinone molecules, J. Phys. Chem. A 115 (2011) 11589–11593.
[44] H.V. Tran, B. Piro, S. Reisberg, L. Huy Nguyen, T. Dung Nguyen, H.T. Duc, et al., An electrochemical ELISA-like immunosensor for miRNAs detection based on screen-printed gold electrodes modified with reduced graphene oxide and carbon nanotubes, Biosens. Bioelectron. 62 (2014) 25–30.
[45] B. Liang, X. Guo, L. Fang, Y. Hu, G. Yang, Q. Zhu, et al., Study of direct electron transfer and enzyme activity of glucose oxidase on graphene surface, Electrochem. Commun. 50 (2015) 1–5.
[46] S. Krishnamurthy, I.V. Lightcap, P.V. Kamat, Electron transfer between methyl viologen radicals and graphene oxide: reduction, electron storage and discharge, J. Photochem. Photobiol. A 221 (2011) 214–219.
[47] H. Tayefi-Nasrabadi, E. Keyhani, J. Keyhani, Conformational changes and activity alterations induced by nickel ion in horseradish peroxidase, Biochimie 88 (2006) 1183–1197.
[48] V.F. Ximenes, L.H. Catalani, A. Campa, Oxidation of melatonin and tryptophan by an HRP cycle involving compound III, Biochem. Biophys. Res. Commun. 287 (2001) 130–134.
[49] L. Wang, A. Lu, T. Lu, X. Ding, X. Huang, Interaction between lanthanum ion and horseradish peroxidase in vitro, Biochimie 92 (2010) 41–50.
[50] Y. Sawada, T. Iyanagi, I. Yamazaki, Relation between redox potentials and rate constants in reactions coupled with the system oxygen–superoxide, Biochemistry 14 (1975) 3761–3764.
[51] Y. Song, G.R. Buettner, Thermodynamic and kinetic considerations for the reaction of semiquinone radicals to form superoxide and hydrogen peroxide, Free Radical Biol. Med. 49 (2010) 919–962.